

<https://doi.org/10.1038/s42005-024-01740-4>

# Broadband optical nonreciprocity by emulation of nonlinear non-Hermitian time-asymmetric loop

Check for updates

Yu Sung Choi<sup>1,2</sup>, Seung Han Shin<sup>1,2</sup>, Seungmin Lee<sup>1,2</sup>, Miji Kim<sup>1</sup> & Jae Woong Yoon <sup>1,2</sup>

Broadband and power-stable optical nonreciprocity is highly desirable for practical implementation of optical isolation of coherent sources and receivers in high-speed data-processing systems. Here, we experimentally demonstrate a  $2 \times 2$  waveguide-coupler system that produces broadband optical nonreciprocity based on simple emulation of nonlinear non-Hermitian time-asymmetric loop. The coupler system consists of five lumped optical components including two linear attenuators and two saturable amplifiers. Under moderate operation conditions which are routinely obtainable with commercial erbium-doped fiber amplifiers, we obtain 20 dB isolation ratio persisting over the entire gain bandwidth of the amplifier and over a wide incident-intensity range from 0.1 mW to 10 kW. The isolation ratio can be enhanced up to 70 dB with the forward transmission efficiency adjustable at any desired stable point by tuning amplifier's internal dissipation in principle. Therefore, our result strongly encourages further experimental development of broadband on-chip optical isolators which have been elusive so far.

Nonreciprocal optical devices including isolators, circulators, and directional amplifiers are indispensable in many optical systems for protecting or stabilizing coherent light sources and detection configurations. Breaking the Lorentz reciprocity of the linear electromagnetism involves magneto-optic media<sup>1–5</sup>, high-frequency temporal modulations<sup>6–14</sup>, and asymmetric Kerr-nonlinear resonances<sup>15–24</sup>.

Each of these approaches has its own advantages and disadvantages in consideration of footprint size, power consumption, integration compatibility, as well as key performance properties including maximally achievable nonreciprocity level, insertion loss, bandwidth, and feasibility under dynamic input scenarios. No single approach can perform the optical isolation superior to the others in all those aspects so far<sup>25–27</sup> and extensive research continues in pursuit of specific application areas for each method.

Toward this end, broadband on-chip optical nonreciprocity was proposed by combining gain-saturation nonlinearity and non-Hermitian adiabatic processes encircling an exceptional point (EP) singularity<sup>28</sup>. In this approach, the desired nonlinear EP-encirclement process is created in a binary coupled-waveguide system with judiciously inter-related modulations in saturable gain and linear loss profiles in two waveguide arms. Intriguingly, 100 THz-wide broadband optical nonreciprocity was theoretically demonstrated. However, its experimental realization still remains elusive because of its structural complexity and the absence of established

fabrication methods creating required gain profiles with acceptably high precision.

In this paper, we experimentally demonstrate that a simple  $2 \times 2$  coupler system emulating the EP-encirclement processes<sup>29</sup> can produce robust optical nonreciprocity if it is combined with gain-saturation nonlinearity. We use fiber-optic attenuators and erbium-doped fiber amplifiers as key elements. Under moderate operation conditions, we obtain 20-dB nonreciprocal transmission ratio (NTR) persisting over the entire gain bandwidth from 1520 to 1570 nm and over a wide incident power range from 0.1 mW to 10 kW. Although we use a fiber-optic system in this proof-of-concept study, our proposed approach can be immediately applicable to monolithic channel waveguide systems based on direct-bandgap semiconductor media. We develop a nonlinear transmission theory of dissipative saturable amplifiers, which quantitatively describes the observed nonreciprocal effects. The theory further implies that the maximally achievable NTR in our system with a commercial attenuators and EDFAs can go up to 70 dB with the forward transmission efficiency adjustable at any desired level below the small-signal gain coefficient by tuning strength of amplifier's internal dissipation. Therefore, we confirm in both theory and experiment that our proposed approach produces robust broadband optical nonreciprocity that might be immediately applicable for producing on-chip broadband optical nonreciprocity on practical integration platforms including CMOS-compatible III-V compound semiconductors.

<sup>1</sup>Department of Physics, Hanyang University, Seoul, 04763, Korea. <sup>2</sup>Research Institute for Natural Sciences, Hanyang University, Seoul, 04763, Korea.

e-mail: [jaeong.yoon@gmail.com](mailto:jaeong.yoon@gmail.com)

**Results**

**Experiment**

We consider a  $2 \times 2$  coupler system consisting of one passive coupler ( $\kappa$ ), two attenuators ( $A_1$  and  $A_2$ ) and amplifiers ( $G_1$  and  $G_2$ ) in diagonal arrangement, as illustrated in Fig. 1a. This coupler configuration was previously suggested by Khurgin et al.<sup>29</sup> as a system emulating dynamic exceptional-point (EP) encirclement processes<sup>30</sup>. Therein, inter-port transmission through the coupler emulates the inter-eigenstate transfer for an EP encirclement process where the final dynamic state is dominated by a preferred adiabatic state with least loss or maximal gain, regardless of any selected initial-state condition.

In this coupler configuration, the transmitted intensity distribution is dominated at the output port with minimal attenuation or maximal amplification, *i.e.*, port  $R_1$  for the forward transmission or port  $L_2$  for the backward transmission in Fig. 1a, regardless of any selected input intensity distribution. This is an effective emulation of asymmetric mode transfer action in the dynamic EP encirclement as we explain below.

Following the previous approaches, we consider non-Hermitian Hamiltonian

$$\mathbf{H} = \begin{bmatrix} p + iq & 1 \\ 1 & -p - iq \end{bmatrix}, \quad (1)$$

which has an exceptional point at  $(p,q) = (0,1)$ .  $\mathbf{H}$  implies a complex eigenvalue spectrum forming a self-intersecting Riemann-sheet geometry indicated in Fig. 1b, c. The wire-frame surface represents the real eigenvalue

$\text{Re}(E)$  while its skin color denotes the imaginary eigenvalue  $\text{Im}(E)$ . A dynamic state evolution in the adiabatic limit follows unusual but simple rules – A dynamic state in the gain mode (eigenstate on the red sheet) evolves in a completely adiabatic manner; A dynamic state in the loss mode (eigenstate on the blue sheet) inevitably undergoes an anti-adiabatic jump towards the gain mode. These rules result in time-asymmetric mode transfer as indicated by arrowed curves in Fig. 1b, c.

Such mode-transfer properties can be better illustrated in a flattened representation of the circular parametric cylinder on  $p$ - $q$  plane, as shown in Fig. 1d, e. Therein, state A is always a preferred final state regardless of initial state selection for the anti-clockwise encirclement, as shown in Fig. 1d. For the clockwise encirclement, state B is always a preferred final state regardless of initial state selection.

The mode transfer property in this particular way is reproduced in the proposed coupler system as illustrated in Fig. 1f, g. States A and B at the endpoints correspond in the same arrangement to channel signals at the input and output terminals of the coupler system. For the forward transmission in analogy to the anti-clockwise EP encirclement in Fig. 1b,  $R_1$  is always a dominant-power output channel regardless of input channel selection. This is readily understood because, on the right side of the coupler, amplifier  $G_1$  amplifies the signal at  $R_1$  while attenuator  $A_2$  suppresses the incoming signal at  $R_2$ . This channel-selected amplification effectively corresponds to the anti-adiabatic jump that induced by mode-selective amplification. In the same manner, channel  $L_2$  is always a dominant-power output channel for the backward transmission case regardless of input channel selection, as shown in Fig. 1c. Therefore, this coupler system

**Fig. 1 | Simple coupler configuration emulating the time-asymmetric mode transfer in EP-encirclement processes.** a Schematic of a  $2 \times 2$  fiber-optic amplifier system that emulates nonlinear dynamic EP encirclement. In a similar manner to the nonlinear dynamic EP-encircling processes, this system can induce strong and robust nonreciprocity due to a combination effect of asymmetric transmission and gain-saturation nonlinearity of erbium-doped fiber amplifiers (EDFA)  $G_1$  and  $G_2$ . b, c Complex eigenvalue spectra of the Hamiltonian in Eq. (1) and dynamic state passages from initial states A and B for anti-clockwise and clockwise EP-encirclement, respectively. d, e Flattened dynamic state passages in (b) and (c). f, g Effective emulation of the dynamic state passages for anti-clockwise and clockwise in the proposed coupler configuration (a).

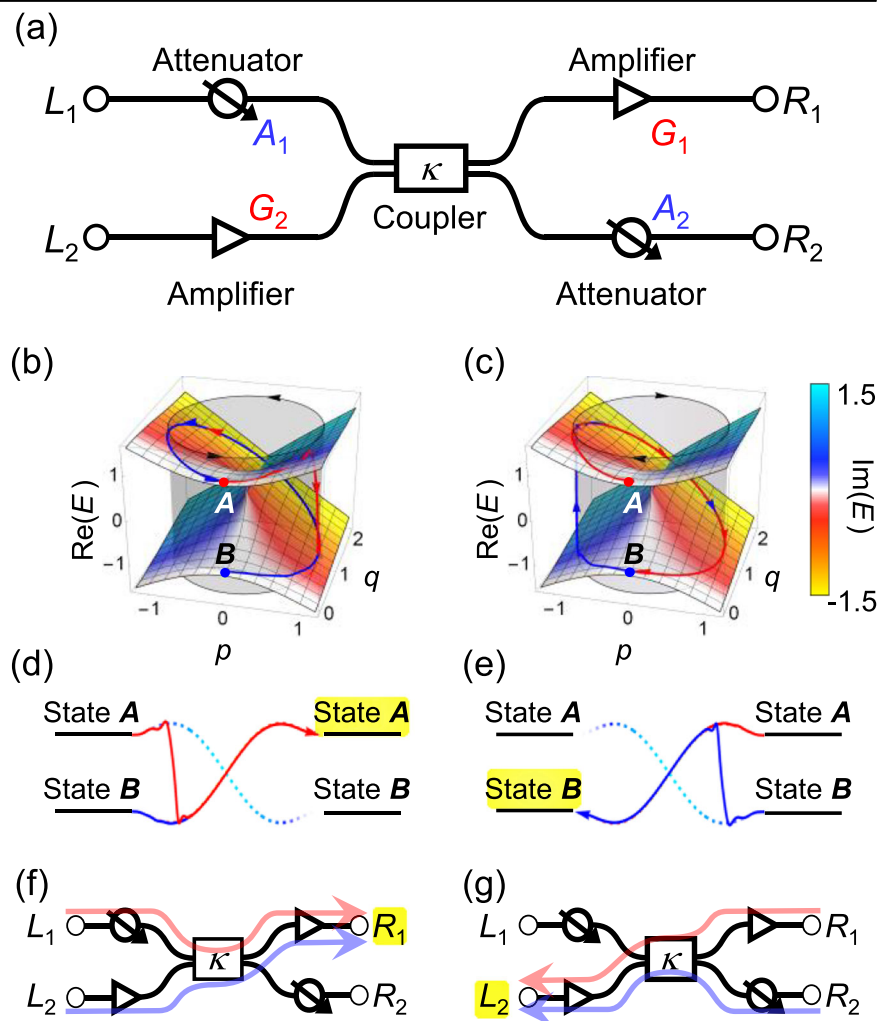
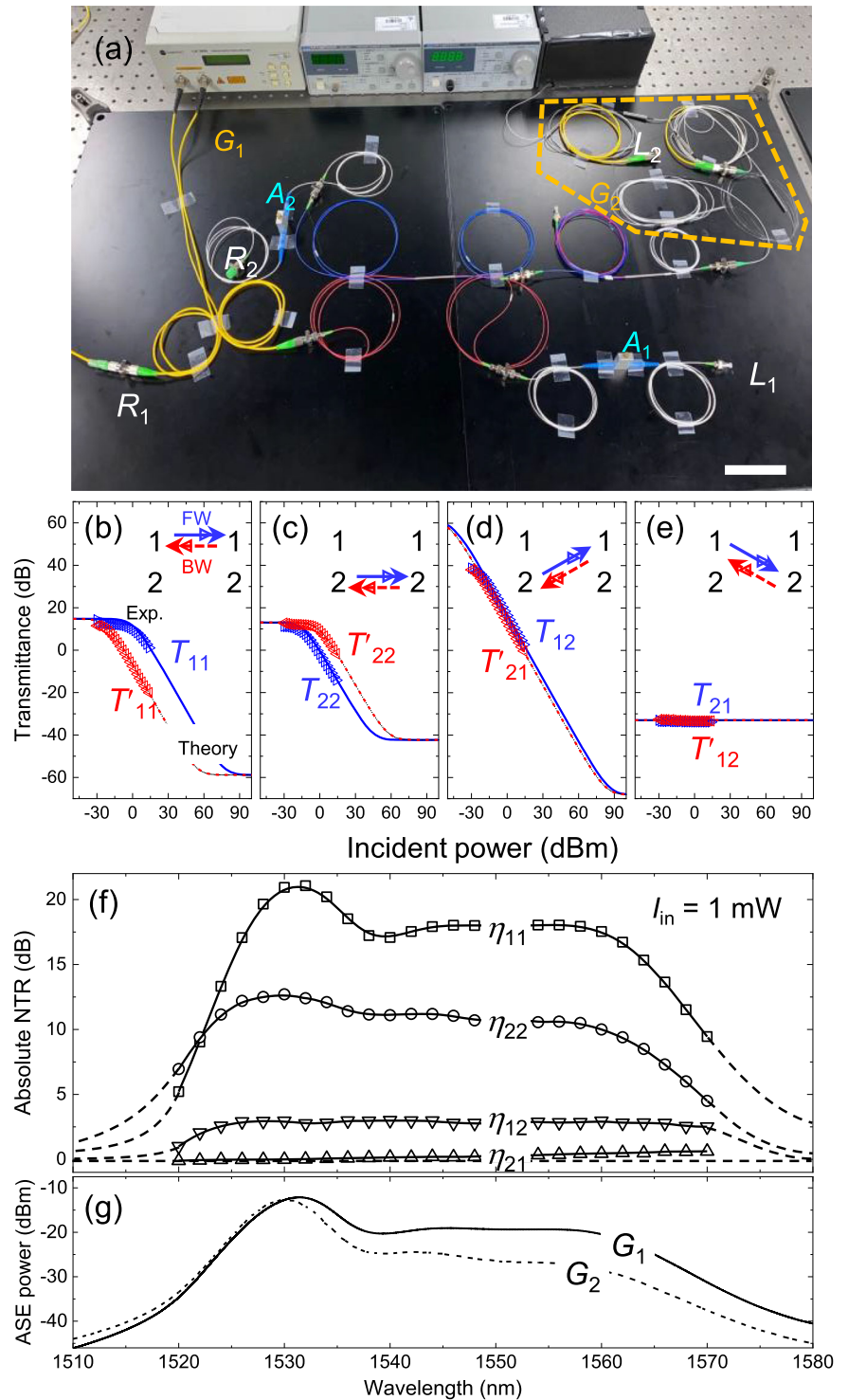


**Fig. 2 | Experimental realization of a non-reciprocal coupler system emulating a nonlinear exceptional-point (EP) encirclement.**  
**a** Experimental realization of the configuration in Fig. 1. **a** Scale bar, 10 cm. **b ~ e** Measured forward and backward transmittances  $T_{nm}$  and  $T'_{mn}$  depending on incident power, where  $n$  and  $m$  are input and output port indices, respectively. Symbols are experimental data and lines are theoretical data for comparison. Details regarding the error bars are provided in the Supplementary Note 1. **f** Absolute nonreciprocal transmission ratio (NTR)  $|\log(T_{nm}/T'_{mn})|$  spectrum over the EDFA gain band from 1510–1580 nm. **g** Amplified spontaneous emission (ASE) spectra of EDFAs  $G_1$  and  $G_2$ , confirming the effective gain band of our analyzed system.



emulates the time-asymmetric mode transfer effect by the dynamic EP encirclement without intricate action of a carefully configured time-varying non-Hermitian Hamiltonian.

In the previous study, the experimental demonstration was performed in the absence of the amplifiers and the asymmetric transmission properties was obtained in the linear, reciprocal regime. In our study here, we include erbium-doped fiber amplifiers (EDFA) and experimentally investigate how the asymmetric port-transmission properties and combined gain-saturation nonlinearity produce the desired nonreciprocal transmission effect.

We construct the system as shown in Fig. 2a. See Methods section for details. Under a condition at  $A_1 = 0.01$ ,  $A_2 = 0.1$ , pump current values

350 mA for  $G_1$  and 250 mA for  $G_2$ , we measure input-power dependent transmittance  $T_{mn} = R_m/L_n$  for the forward transmission and  $T'_{mn} = L_m/R_n$  for the backward transmission, as shown in Fig. 2b–e. Note therein that  $T_{mn}$  and  $T'_{mn}$  are a time-reversal pair and we compare each pair in a single graph. In these graphs, triangular symbols indicate experimental data in comparison with theoretical curves due to a simplified model of a dissipative saturable amplifier, which we will explain in the next section. Error bars are omitted in the main figures as the measurement errors are sufficiently small compared to the symbol size. See Supplementary Fig. S1 in Supplementary Note 1. Therein, we estimate average standard deviation in the measured power  $\sim 0.02$  dB with the maximum value 0.6 dB, which is merely a sub 1%

magnitude. The errors in the power are dominantly from the spontaneous emission noises in the EDFA. The nonreciprocal transmission appears as deviation of  $T_{mn}$  from  $T'_{nm}$ . Strong nonreciprocity over a wide input-power range from 0.1 mW to 1 kW at 1,550 nm wavelength is obtained for the straight-through pairs of  $T_{11}$ - $T'_{11}$  in Fig. 2b and  $T_{22}$ - $T'_{22}$  in Fig. 2c. In contrast, weak nonreciprocity is observed for  $T_{12}$ - $T'_{21}$  in Fig. 2d over a wide incident power range, while  $T_{21}$ - $T'_{12}$  in Fig. 2e, composed of linear attenuators, is confirmed to be reciprocal.

The strong nonreciprocity for the straight-through pairs are persistent over the entire gain bandwidth of the EDFAs from 1,520 to 1,570 nm, as shown in Fig. 2(f) for the nonreciprocal transmission ratio (NTR)  $\eta_{mn} = T_{mn}/T'_{nm}$  spectra in comparison with Fig. 2g for the amplified spontaneous emission (ASE) spectra of  $G_1$  and  $G_2$  EDFAs. In particular, straight-through NTRs  $\eta_{11}$  and  $\eta_{22}$  at the gain-peak wavelength of the EDFAs around 1,530 nm go beyond 20 and 10 dB, respectively. We note that the peak NTR value in this experimental condition can be largely increased up to  $\sim 70$  dB according to our theory providing the experimentally consistent theoretical curves in Fig. 2b–e.

The observed broadband nonreciprocal transmission effect can be understood in analogy to the nonlinear EP-encirclement processes<sup>22</sup> because this emulating coupler system has the two essential properties in common. They are the time-asymmetric mode transfer and gain-saturation nonlinearity. Although the emulating coupler system does not involve intricate nonlinear dynamic state evolution for the EP-encirclement processes, our proposed system might produce more robust nonreciprocity and allows simpler theoretical description of the key performance properties such as peak NTR, maximally achievable NTR limit, and nonreciprocal input-power range, as we will explain in the next section.

### Theory

The observed nonreciprocal transmission effect in Fig. 2 reveals several major features as summarized below.

- (A) Nonreciprocity appears only for the straight-through transmission pairs while the cross transmission pairs  $T_{mn}$ - $T'_{nm}$  ( $m \neq n$ ) are almost or strictly reciprocal.
- (B) There is an upper bound in the incident-power window for the nonreciprocal transmission, implying that high input-power does not necessarily guarantee the nonreciprocity even though stronger gain-saturation nonlinearity is activated.
- (C) The peak NTR value is in the order of attenuation coefficient  $A_n$  of the linear attenuator in the corresponding transmission path.

In order to conveniently describe these experimental features, we express the forward ( $\mathbf{T}$ ) and backward ( $\mathbf{T}'$ ) scattering matrix in terms of  $A_n$  and  $G_n$  as

$$\mathbf{T} = \begin{bmatrix} T_{11} & T_{12} \\ T_{21} & T_{22} \end{bmatrix} = \begin{bmatrix} \kappa_t A_1 G_1(J_3) & \kappa_x G_2(I_2) G_1(J_3) \\ \kappa_x A_1 A_2 & \kappa_t G_2(I_2) A_2 \end{bmatrix}, \quad (2)$$

$$\mathbf{T}' = \begin{bmatrix} T'_{11} & T'_{12} \\ T'_{21} & T'_{22} \end{bmatrix} = \begin{bmatrix} \kappa_t G_1(I_3) A_1 & \kappa_x A_1 A_2 \\ \kappa_x G_1(I_3) G_2(J_2) & \kappa_t A_2 G_2(J_2) \end{bmatrix}, \quad (3)$$

where  $I_i$  is incident optical power at channel  $i = 1$  ( $L_1$ ), 2 ( $L_2$ ), 3 ( $R_1$ ), and 4 ( $R_2$ ).  $\kappa_t$  and  $\kappa_x$  represent straight-through ( $n$ -to- $n$ ) and cross ( $n$ -to- $m$ ,  $n \neq m$ ) power-coupling efficiencies at the central passive coupler, respectively.  $J_3$  in Eq. (2) is optical power coupled toward  $R_1$  at the central coupler, while  $J_2$  in Eq. (3) is optical power coupled toward  $L_2$  at the coupler, which takes expressions

$$J_3 = \kappa_t A_1 I_1 + \kappa_x G_2(I_2) I_2, \quad (4)$$

$$J_2 = \kappa_x G_1(I_3) I_3 + \kappa_t A_2 I_4. \quad (5)$$

Forward to backward NTR calculated from the scattering matrices in Eqs. (2) and (3) gives

$$\eta_{11} = \frac{T_{11}}{T'_{11}} = \frac{G_1(\kappa_t A_1 I_{in})}{G_1(I_{in})}, \quad (6)$$

$$\eta_{12} = \frac{T_{12}}{T'_{21}} = \frac{G_2(I_{in}) G_1(\kappa_x G_2(I_{in}) I_{in})}{G_1(I_{in}) G_2(\kappa_x G_1(I_{in}) I_{in})}, \quad (7)$$

$$\eta_{21} = \frac{T_{21}}{T'_{12}} = 1, \quad (8)$$

$$\eta_{22} = \frac{T_{22}}{T'_{22}} = \frac{G_2(I_{in})}{G_2(\kappa_t A_2 I_{in})}, \quad (9)$$

where incident power  $I_{in}$  is identical for the forward and backward transmission, attenuator responses are linear and thereby  $A_n$  is independent of input power, and amplifiers are nonlinear and subsequently their amplification coefficient  $G_n(I_0)$  basically depends on input optical power  $I_0$  at the amplifier.

The reciprocal nature of the crossover transmission is easily understood. Crossover NTR  $\eta_{21}$  in Eq. (8) is always unity (reciprocal) because the corresponding transmission pathway involves only passive linear components  $A_1$  and  $A_2$ . In addition, the other crossover NTR  $\eta_{12}$  in Eq. (7) represents weak nonreciprocity although two nonlinear amplifiers  $G_1$  and  $G_2$  are included in the pathway. This is because  $\eta_{12}$  essentially reduces to unity if the two amplifiers are identical, *i.e.*,  $\eta_{12} = 1$  for  $G_1 = G_2$ . Slight nonreciprocity of  $\eta_{12}$  in Fig. 2(e) is because  $G_1 \neq G_2$  in our experiment.

Strong nonreciprocity ( $\eta_{pq} \gg 1$  or  $\eta_{pq} \ll 1$ ) is expected only for the straight-through transmission ( $\eta_{11}$  and  $\eta_{22}$ ) in Eqs. (6) and (9). For the straight-through transmission, the sequential order of the attenuator and amplifier actions experienced by the optical signal are reversed between two reciprocal cases and the difference in the nonlinear amplifier gain can be made. For the straight-through NTR,  $\eta_{mn}$  is determined simply by a ratio of the amplifier gain coefficients as

$$\rho_n = \frac{G_n(\kappa_t A_n I_{in})}{G_n(I_{in})}. \quad (10)$$

This nonreciprocal gain ratio is related to the straight-through NTR such that  $\eta_{11} = \rho_1$  and  $\eta_{22} = \rho_2^{-1}$ . Therefore, a crucial part of the theoretical understanding is a description of the nonlinear gain-coefficient  $G_n$  as a function of input optical power  $I_0$ .

We use a dissipative saturable-amplifier model for  $G_n(I_0)$ . In this model, we assume a standard saturable-gain constant

$$\Gamma_n(z) = \frac{\gamma_n}{1 + I(z)/I_{sn}}, \quad (11)$$

where  $\gamma_n$  is small-signal gain constant,  $I(z)$  is local power of the optical signal at position  $z$  along the optical axis of the EDFA,  $I_{sn}$  is saturation-power constant, and subscript  $n$  is port index. Amplification of  $I(z)$  is described by a nonlinear equation as

$$\frac{dI(z)}{dz} = [\Gamma_n(z) - \alpha_n] I(z), \quad (12)$$

where  $\alpha_n$  is internal dissipation rate which is caused primarily by a diffuse scattering of the optical signal through the stimulated absorption and subsequent stimulated emission of the  $\text{Er}^{3+}$  ions to the ASE noise. See Supplementary Note 2 for  $\alpha_n$  measured in our experiment as a function of pump and input optical powers, which confirms the ASE-noise-dominant internal dissipation of the EDFA.

Equation (12) yields nonlinear gain coefficient  $G_n = I(d)/I(0)$  for a given EDFA length  $d_n$  to be determined as

$$\ln G_n = \ln G_n^{(0)} - \frac{\gamma_n}{\alpha_n} \ln \left[ \frac{I_{cn}/I_0 - 1}{I_{cn}/I_0 - G_n} \right], \quad (13)$$

where  $G_n^{(0)} = \exp[(\gamma_n - \alpha_n)d_n]$  is small-signal gain coefficient which is the special solution of  $G_n$  in the low-power limit of  $I(0 \leq z \leq d_n) \ll I_{sn}$ ,  $I_0 = I(0)$  is input power, and  $I_{cn} = I(\infty) = (\gamma_n/\alpha_n - 1)I_{sn}$  is clamping-power constant that represents output power for an infinitely long amplifier ( $d_n = \infty$ ). Note that finite  $I_{cn}$  is a unique feature of a dissipative saturable amplifier. For lossless saturable amplifiers ( $\alpha_n = 0$ ) in contrast,  $I_{cn} \rightarrow \infty$  because the local optical power is amplified in a non-exponential linear fashion even if the gain is fully saturated, i.e.,  $I(z) \sim \gamma_n z I_{sn}$  according to Eq. (12) for the very-high intensity limit ( $I \gg I_{sn}$ ).

We show a typical profile of  $G_n(I_0)$  as a function of input power  $I_0$  in Fig. 3a. There are three characteristic  $I_0$  domains as

$$G_n(I_0) \approx \begin{cases} \exp[(\gamma_n - \alpha_n)d_n] & (I_0 \ll I_s) \\ I_{cn} / I_0 & (I_0 \approx I_s) \\ \exp(-\alpha_n d_n) & (I_0 \gg I_s) \end{cases}. \quad (14)$$

In the low  $I_0$  limit ( $I_0 \ll I_{sn}$ ),  $G(I_0)$  is constant at  $G_n^{(0)} = \exp[(\gamma_n - \alpha_n)d_n]$  because the gain-saturation nonlinearity is not activated. Hence the amplifier acts as a linear amplifier. Consequently, response of the system is linear and reciprocal.

In the high  $I_0$  limit ( $I_0 \gg I_{sn}$ ),  $G(I_0)$  is also constant at another lower level  $\exp(-\alpha_n d_n)$  and thereby response of the amplifier is linear in spite of strong activation of the gain saturation nonlinearity. This is because gain constant  $\Gamma_n$  in Eq. (11) becomes negligible and the amplifier acts as a linear attenuator with attenuation rate  $\alpha_n$ . Therefore, the coupler system is linear and reciprocal again in the high  $I_0$  limit.

Strong  $I_0$  dependence of the amplifier gain coefficient is obtained in the intermediate intensity region ( $I_0 \approx I_{sn}$ ).  $G(I_0 \approx I_{sn}) \approx I_{cn}/I_0$  in Eq. (14) is a fairly good approximation as shown in Fig. 3a. In Fig. 3a, the nonlinear gain-coefficient window is identified as  $I_{low} < I_0 < I_{high}$ , where the lower and upper bounds are

$$I_{low} \approx I_{cn}/G^{(0)} = I_{sn}(\gamma_n/\alpha_n - 1) \exp[(\alpha_n - \gamma_n)d_n], \quad (15)$$

$$I_{high} \approx I_{sn}(\gamma_n/\alpha_n - 1) \exp(\alpha_n d_n), \quad (16)$$

yielding their ratio  $I_{high}/I_{low} \approx \exp(\gamma_n d_n)$ . Taking into account the non-reciprocal gain ratio  $\rho_n$  in Eq. (10), the nonreciprocal transmission is obtained if this nonlinear gain-coefficient window is in between two input-intensity points  $I_0 = \kappa_t A_n I_{in}$  and  $I_{in}$ .

The key performance properties such as peak NTR and nonreciprocal input-intensity range (NRIR) can be conveniently inferred from the features revealed in Fig. 3a.

There are four cases that nonreciprocity is obtained, as graphically explained in Fig. 3b. In Case I, incident power  $I_{in}$  (bare input) is within the nonlinear gain window while the attenuated input power  $\kappa_t A_n I_{in}$  stays within the low-power linear-amplifier range. The nonreciprocal gain ratio in this case is  $\rho_n \approx G_n^{(0)}(I_{in}/I_{cn}) = I_{in}[I_{sn}(\gamma_n/\alpha_n - 1)]^{-1} \exp[(\alpha_n - \gamma_n)d_n]$ . Therefore, the NTR linearly increases with  $I_{in}$ .

Increase in  $I_{in}$  from Case I leads to Case II where both bare input power  $I_{in}$  and attenuated input power  $\kappa_t A_n I_{in}$  are within the nonlinear gain window. In this case,  $\rho_n \approx (\kappa_t A_n)^{-1}$ , implying that the NTR is inversely proportional to attenuation coefficient  $A_n$  of the attenuator. We note that Case II happens only if the value of  $A_n$  is moderate such that ratio  $I_{in}/(\kappa_t A_n I_{in}) = (\kappa_t A_n)^{-1}$  of the bare and attenuated input powers is smaller than ratio  $I_{high}/I_{low} = \exp(\gamma_n d_n)$ . This condition for Case II can be simply written by  $(\kappa_t A_n)^{-1} < \exp(\gamma_n d_n)$ . The approximate gain-coefficient expressions in Eq. (14) leads to  $\rho_n \approx (\kappa_t A_n)^{-1}$  as the peak NTR for Case II with the moderate-attenuation condition.

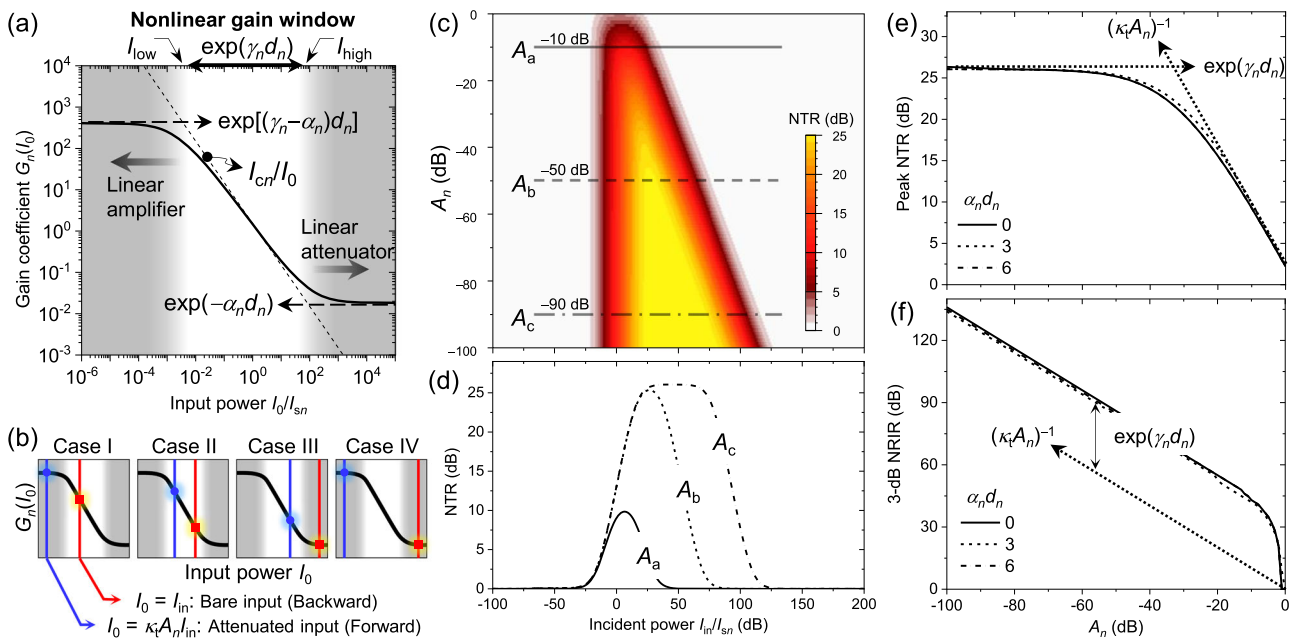


**Fig. 3 | Theoretical model for the observed nonreciprocal transmission.** **a** Nonlinear gain coefficient of a dissipative amplifier due to Eq. (11) as a function of input power  $I_0$  relative to saturation-intensity constant  $I_{sn}$ . Parameter conditions are  $\gamma_n d_n = 10$ ,  $\alpha_n d_n = 4$ . **b** Schematic illustration of four necessary cases showing nonreciprocity, based on the relative positions of bare input power and attenuated input power with respect to the amplifier's nonlinear gain window. **c** Typical nonreciprocal transmission ratio (NTR) map on  $I_{in}$ - $A_n$  plane.  $I_{in}$  and  $A_n$  represent

incident intensity and attenuation coefficient of the attenuator in Fig. 1a. Parameter conditions are  $\gamma_n d_n = 6$ ,  $\alpha_n d_n = 3$ , and  $\kappa_t = 0.5$ . **d** NTR profile for three selected  $A_n$  conditions at  $A_a = -10$  dB,  $A_b = -50$  dB, and  $A_c = -90$  dB. These three conditions are indicated by horizontal lines in (c). **e** Peak NTR dependence on  $A_n$  for different internal-dissipation conditions at  $\alpha_n d_n = 0, 3$ , and  $6$ . **f** Nonreciprocal input-power range for 3-dB-NTR threshold as a function of  $A_n$  for  $\alpha_n d_n = 0, 3$ , and  $6$ .

Further increase in  $I_{in}$  beyond the upper nonlinear gain window results in Case III where attenuated input power  $\kappa_n A_n I_{in}$  is still within the nonlinear gain window. In this case,  $\rho_n \approx (I_{cn}/I_{in}) \exp(\alpha_n d_n) = I_{in}^{-1} [I_{sn}(\gamma_n/\alpha_n - 1)] \exp(\alpha_n d_n)$  and thereby the NTR inversely proportional to  $I_{in}$ .

The NTR reaches its maximally possible limit in this high  $I_{in}$  condition when the attenuation is very strong such that  $(\kappa_n A_n)^{-1} > \exp(\gamma_n d_n)$ . This situation corresponds to Case IV in Fig. 3b. In this high-incident-power and strong-attenuation condition,  $I_{in}$  stays in the high-power, linear-attenuator range while the attenuated input power  $\kappa_n A_n I_{in}$  is in the low-power, linear-amplifier range. The nonreciprocal gain ratio, or equivalently the NTR, is constant at  $\rho_n \approx \exp(\gamma_n d_n)$  and this level is the maximally-obtainable limit for the peak NTR.

The NRIR can also be conveniently inferred from these arguments based on the nonlinear gain-coefficient property in Fig. 3a, b. In Table 1, we summarize the NRIR and peak NTR expressions depending on the attenuation coefficient  $A_n$  as the key conditioning parameter.

These approximate expressions properly describe the major NTR properties revealed in a two-dimensional map on  $I_{in}$ - $A_n$  plane as shown in Fig. 3c as an exemplary case. The domain of NTR is in triangular shape with the peak NTR is saturated at  $\sim 25$  dB consistent with a value of  $\exp(\gamma_n d_n) = 26$  dB. The NRIR lower bound is constant at  $\sim 10^{-2} I_{sn}$  while the upper bound increases with  $A_n^{-1}$  as predicted from the expressions in Table 1. In Fig. 3d, we indicate the NTR profiles for three selected  $A_n$  values at  $-10$ ,  $-50$ , and  $-90$  dB in order to see how the  $I_{in}$ -dependent profile changes with increasing attenuation strength  $A_n^{-1}$  according to our suggested theory. Dependences of the peak NTR and NRIR on  $A_n^{-1}$  are shown in Fig. 3e, f. They are consistent with the approximate expressions in Table 1. We note that the peak NTR and NRIR do not depend on internal dissipation  $\alpha_n d_n$  of the EDFA even for an extreme case of  $\alpha_n d_n = 6 = \gamma_n d_n$ , at which the amplifier operates in an attenuation mode over the entire input-intensity range.

Considering features associated with output intensity clamping at  $I_{cn} = (\gamma_n/\alpha_n - 1)I_{sn}$  for dissipative amplifiers, deliberate inclusion of internal dissipation  $\alpha_n$  can be used for efficiently adjusting output power level at a certain desired value without any degradation in the nonreciprocal transmission properties. For lossless amplifiers, the output power level is also tunable by means of  $\gamma_n$  control. However, change in  $\gamma_n$  immediately alter the key performance properties such as the NRIR width and peak NTR.

We finally compare our proposed theory with experiments. In Fig. 4a, gain coefficient measurement data for  $G_1$  and  $G_2$  are indicated in comparison with the theoretical fitting curves. The EDFA conditions in experiment are identical to those for Fig. 2b ~ 2(g). The optimized parameters for the best fit are used to calculate the absolute NTR  $\eta_{nm}$  profile on the incident-intensity ( $I_{in}$ ) domain and compared with the experimental data, as shown in Fig. 4b. The measured data are quantitatively consistent with the theory for all four input and output port combinations, confirming the validity of our proposed theory and its predicted robustness of the nonreciprocity implied in Fig. 3.

We note that the theoretical curves imply an extremely wide NRIR from 0.1 mW – 10 kW with our moderate experimental conditions. Although the peak NTR  $\sim 22$  dB is high enough to be used in practice, it can be greatly enhanced up to  $\sim 74$  dB in principle. In the measured cases, the

system is operating obviously in the weak attenuation limit because  $(\kappa_n A_n)^{-1} = 23$  dB  $\ll \exp(\gamma_n d_n) = 73.6$  dB. Consequently, the peak NTR  $\sim (\kappa_n A_n)^{-1} = 23$  dB and this value can be increased by employing a stronger attenuator. Getting into the strong attenuation limit, the peak NTR approaches  $\exp(\gamma_n d_n) = 73.6$  dB.

### Discussion

We have experimentally realized a nonreciprocal 2x2 fiber-optic coupler system that emulates dynamic nonlinear EP-encirclement processes. The desired nonlinear non-Hermitian properties are successfully emulated in a simple coupler structure consisting of two passive attenuators, two EDFAs, and one passive coupler. Under moderate operation conditions at pump current  $\sim 300$  mA and attenuation strength  $\sim -20$  dB, Robust nonreciprocal transmission with NTR  $\sim 20$  dB is obtained over a wide input power range from 0.1 mW to 10 kW and within the entire gain bandwidth from 1520 – 1570 nm. We provide a simple theory based on a dissipative saturable amplifier, which is quantitatively consistent with the experimental results. The theory further suggests that the NTR can be enhanced up to 70 dB and forward transmission intensity can be adjusted at any arbitrary stable level without any degradation of the nonreciprocity by controlling internal dissipation of the EDFA. Therefore, we confirm in both experiment and theory that EP-encirclement emulation combined with gain-saturation non-linearity creates robust nonreciprocity.

In further consideration for the follow-up study, it is of special interest to investigate whether the proposed system is capable of activating dynamic nonreciprocity. Dynamic nonreciprocity is obtained when nonreciprocity in the transmission exists for simultaneous forward and backward inputs, and is crucial for practical implementation of general-purpose optical isolators<sup>27,31,32</sup>. In linear nonreciprocal systems based on magneto-optic crystals<sup>1-5</sup> and time-varying index approaches<sup>6</sup>, dynamic nonreciprocity is naturally activated without any additional conditions. In contrast, the nonlinear nonreciprocity demands special restrictions because the transmission properties change with field strength and spatial/spectral distributions, as pointed out in ref. 32. In further detail, self-phase modulation effect due to Kerr nonlinearity does not activate the dynamic nonreciprocity. Intriguingly, it turned out that the nonlinear dynamic nonreciprocity is feasible with cross-phase modulation effect from Kerr nonlinearity but it is available only within a narrowly limited intensity condition<sup>20</sup>. For gain-saturation or saturable-absorption nonlinearity, it is still unclear whether they are capable of producing dynamic nonreciprocity or not, and it is a subject of extensive further study.

In our proposed system, dynamic nonreciprocity seems unlikely when we consider some limiting cases. In the infinitely-long-amplifier limit, output power of the amplifier is always clamped at a fixed level of  $I_{cn}$ . This property corresponds to the  $I_{cn}/I_0$  line in the gain coefficient curve in Fig. 3a. Once this condition is accomplished for a specific  $L_n$ - $R_n$  path, forward output power through the path is  $I_{cn}$  regardless of input power whereas the backward output power is clamped at  $(1-\kappa^2)A_n I_{cn}$ . Therefore, we obtain nonreciprocity with NTR  $\sim [(1-\kappa^2)A_n]^{-1}$  regardless of input power in the infinitely-long-amplifier limit. Now, we further consider simultaneous small forward and backward signals added in the presence of pre-existing high-power forward signals. As the forward and backward output power is

**Table 1 | Approximate expressions of nonreciprocal input-power range (NRIR) and peak nonreciprocal transmission ratio (NTR)**

Attenuation strength	Peak NTR	Nonreciprocal input-power range (NRIR)		
		Lower bound $[I_{in}]_{min}$	Upper bound $[I_{in}]_{max}$	Ratio $[I_{in}]_{max}/[I_{in}]_{min}$
$(\kappa_n A_n)^{-1} < \exp(\gamma_n d_n)$ Weak attenuation limit	$(\kappa_n A_n)^{-1}$	$I_{cn} \exp[(a_n - \gamma_n) d_n]$	$I_{cn} \exp(a_n d_n) (\kappa_n A_n)^{-1}$	$\exp(\gamma_n d_n) (\kappa_n A_n)^{-1}$
$(\kappa_n A_n)^{-1} > \exp(\gamma_n d_n)$ Strong attenuation limit	$\exp(\gamma_n d_n)$			

Note the definitions of the variables as  $\kappa_n$  – straight-through power-coupling constant at the central passive coupler,  $A_n$  – attenuation coefficient of the attenuator at channel  $n$ ,  $\gamma_n$  – small-signal gain constant of the EDFA amplifier at channel  $n$ ,  $\alpha_n$  – internal dissipation rate of the EDFA amplifier at channel  $n$ ,  $d_n$  – length of the EDFA amplifier at channel  $n$ ,  $I_{cn}$  – clamping intensity constant of the EDFA amplifier at channel  $n$ .

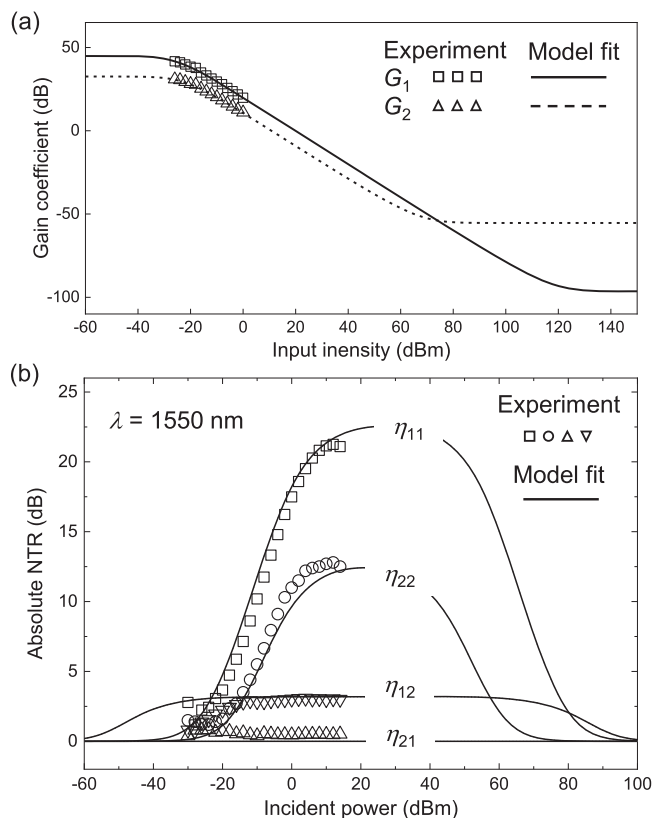


**Fig. 4 | Consistency of the theory with experiment.** **a** Gain coefficient profiles for parametric fitting of  $\gamma_n$  and  $\alpha_n$  of  $G_n$ . The best fits indicated by the solid and dashed curves are provided by parameters  $\gamma_1 = 0.113 \text{ cm}^{-1}$  and  $\alpha_1 = 0.055 \text{ cm}^{-1}$  for  $G_1$  and  $\gamma_2 = 0.085 \text{ cm}^{-1}$  and  $\alpha_2 = 0.045 \text{ cm}^{-1}$  for  $G_2$ . Amplifier lengths are  $d_1 = d_2 = 1.5 \text{ m}$ . **b** Comparison of the NTR  $\eta_{nm}$  for all four input and output port combinations between the theory and experiment at wavelength 1,550 nm.

clamped at fixed levels of  $I_{cn}$  and  $(1-\kappa^2)A_n I_{cn}$ , respectively, any additional inputs at the forward and backward channels cannot transmit through the system, implying dynamic reciprocity. Nevertheless, there might be certain parametric conditions for the dynamic nonreciprocity in certain non-limiting case scenarios and we consider that it should be further studied in the future.

Although the dynamic nonreciprocity does not seem plausible, our proposed system can be useful as a laser protection or intensity stabilization device. Following the argument for the infinitely-long-amplifier limit, any drift in the forward signal does not transmit, meaning that the coupler operates as an intensity stabilizer. In addition, laser protection requires suppression of backward waves at a certain minimum level in their absolute intensity, not transmittance value. If the backward clamping power  $(1-\kappa^2)A_n I_{cn}$  is lower than the required minimum level, the coupler system provides the protection simultaneously with the forward power stabilization. Considering the simplicity in the structure configuration and robustness in the nonreciprocal properties of our proposed system, on-chip implementation based on III-V compound semiconductor platforms is definitely of special interest for realizing broadband on-chip laser-protection and stabilization devices.

## Methods

We use a commercial EDFA (LXI 2000, Luxper Technologies) for  $G_1$ , a custom-built EDFA for  $G_2$ , and commercial variable attenuators (VOA50, Thorlabs) for  $A_1$  and  $A_2$ . In our description hereafter, we take  $G_n$  and  $A_n$  as respectively representing gain and attenuation coefficients, which are defined by an optical power ratio of the output to the input at the corresponding element.

When measuring the transmission between two ports, only the amplifier within the transmission path is pumped. For the  $T_{11}$  and  $T_{11}'$  measurement,  $G_1$  is pumped at 350 mA while  $G_2$  is not pumped. For the  $T_{22}$  and  $T_{22}'$  measurement in contrast,  $G_1$  is not pumped while  $G_2$  is pumped at 250 mA. Consistently, both  $G_1$  and  $G_2$  are simultaneously pumped at 350 and 250 mA, respectively, for the  $T_{12}$  and  $T_{21}'$  measurement. For the  $T_{21}$  and  $T_{12}'$  measurement in contrast, both  $G_1$  and  $G_2$  are not pumped. Therefore, the non-reciprocal pairs are measured in the identical conditions.

At the central coupler, light also couples to the ports that are not being measured. In this transmission passage, back reflection is negligible for following reasons. First, the central coupler is connected through angled physical contact (FC/APC) connector, so that about 4% reflection is extinct from the signal path. We experimentally verify that the reflectance at the port interfaces is  $< -60 \text{ dB}$  (See Supplementary Note 3). Second, any back-reflected light towards the port with an attenuator undergoes attenuation twice. This yields an additional 10 dB or 20 dB reduction of the reflected signal. Finally, a port with EDFA in the reflection path is not pumped and thereby further attenuates reflected light.

## Data availability

The data that support the plots within this paper and other findings of this study are available from the corresponding author upon reasonable request.

Received: 25 December 2023; Accepted: 8 July 2024;

Published online: 03 August 2024

## References

- Asadchy, V. S., Mirmoosa, M. S., Diaz-Rubio, A., Fan, S. & Tretyakov, S. A. Tutorial on electromagnetic nonreciprocity and its origins. *Proc. IEEE* **108**, 1684–1727 (2020).
- Ma, J. et al. Hybrid graphene/silicon integrated optical isolators with photonic spin-orbit interaction. *Appl. Phys. Lett.* **108**, 151103 (2016).
- Grede, A. J., Krainova, N. & Giebink, N. C. Exceptional point magneto-optic isolators. *Opt. Express* **29**, 22614–22622 (2021).
- Zvezdin, A. K. & Kotov, V. A. *Modern Magneto-optics and Magneto-optical Materials* 1st edn, 404 (CRC Press, 1997).
- Ren, S. Y. et al. Single-photon nonreciprocity with an integrated magneto-optical isolator. *Laser Photonics Rev.* **16**, 2100595 (2022).
- Sounas, D. L. & Alù, A. Non-reciprocal photonics based on time modulation. *Nat. Photonics* **11**, 774–783 (2017).
- Nassar, H. et al. Nonreciprocity in acoustic and elastic materials. *Nat. Rev. Mater.* **5**, 667–685 (2020).
- Fan, S., Shi, Y. & Lin, Q. Nonreciprocal photonics without magneto-optics. *IEEE Antennas Wirel. Propag. Lett.* **17**, 1948–1952 (2018).
- Tzuan, L. D., Fang, K., Nussenzeig, P., Fan, S. & Lipson, M. Non-reciprocal phase shift induced by an effective magnetic flux for light. *Nat. Photonics* **8**, 701–705 (2014).
- Kittlaus, E. A., Otterstrom, N. T., Kharel, P., Gertler, S. & Rakich, P. T. Non-reciprocal interband brillouin modulation. *Nat. Photonics* **12**, 613–619 (2018).
- Tian, H. et al. Magnetic-free silicon nitride integrated optical isolator. *Nat. Photonics* **15**, 828–836 (2021).
- Kittlaus, E. A. et al. Electrically driven acousto-optics and broadband non-reciprocity in silicon photonics. *Nat. Photonics* **15**, 43–52 (2021).
- Sohn, D. B., Örsel, O. E. & Bahl, G. Electrically driven optical isolation through phonon-mediated photonic Autler–townes splitting. *Nat. Photonics* **15**, 822–827 (2021).
- Fang, K. et al. Generalized non-reciprocity in an optomechanical circuit via synthetic magnetism and reservoir engineering. *Nat. Phys.* **13**, 465–471 (2017).
- Huang, X., Lu, C., Liang, C., Tao, H. & Liu, Y.-C. Loss-induced nonreciprocity. *Light. Sci. Appl.* **10**, 30 (2021).
- Jiang, X. et al. On-chip optical nonreciprocity using an active microcavity. *Sci. Rep.* **6**, 38972 (2016).

17. Sounas, D. L. & Alu, A. Nonreciprocity based on nonlinear resonances. *IEEE Antennas Wirel. Propag. Lett.* **17**, 1958–1962 (2018).
18. Del Bino, L. et al. Microresonator isolators and circulators based on the intrinsic nonreciprocity of the Kerr effect. *Optica* **5**, 279–282 (2018).
19. Cao, Q.-T. et al. Experimental demonstration of spontaneous chirality in a nonlinear microresonator. *Phys. Rev. Lett.* **118**, 033901 (2017).
20. White, A. D. et al. Integrated passive nonlinear optical isolators. *Nat. Photonics* **17**, 143–149 (2023).
21. Li, E.-Z. et al. Experimental demonstration of cavity-free optical isolators and optical circulators. *Phys. Rev. Res.* **2**, 033517 (2020).
22. Du, Q. et al. Monolithic on-chip magneto-optical isolator with 3 dB insertion loss and 40 dB isolation ratio. *ACS Photonics* **5**, 5010–5016 (2018).
23. Liu, S., Shoji, Y. & Mizumoto, T. TE-mode magneto-optical isolator based on an asymmetric microring resonator under a unidirectional magnetic field. *Opt. Express* **30**, 9934–9943 (2022).
24. Chen, J., Chen, Z., Li, Y., Sun, Q. & Xu, J. Nonreciprocal isolator based on a plasmonic magneto-optical resonator. *Opt. Commun.* **459**, 124953 (2020).
25. Khurgin, J. B. Optical isolation by temporal modulation: size, frequency, and power constraints. *ACS Photonics* **10**, 1037–1045 (2023).
26. Potton, R. J. Reciprocity in optics. *Rep. Prog. Phys.* **67**, 717 (2004).
27. Caloz, C. et al. Electromagnetic nonreciprocity. *Phys. Rev. Appl.* **10**, 047001 (2018).
28. Choi, Y., Hahn, C., Yoon, J. W., Song, S. H. & Berini, P. Extremely broadband, on-chip optical nonreciprocity enabled by mimicking nonlinear anti-adiabatic quantum jumps near exceptional points. *Nat. Commun.* **8**, 14154 (2017).
29. Khurgin, J. et al. Emulating exceptional-point encirclements using imperfect (leaky) photonic components: asymmetric mode-switching and omni-polarizer action. *Optica* **8**, 563–569 (2021).
30. Doppler, J. et al. Dynamically encircling an exceptional point for asymmetric mode switching. *Nature* **537**, 76–79 (2016).
31. Jalas, D. et al. What is—and what is not—an optical isolator. *Nat. Photonics* **7**, 579–582 (2013).
32. Shi, Y., Yu, Z. & Fan, S. Limitations of nonlinear optical isolators due to dynamic reciprocity. *Nat. Photonics* **9**, 388–392 (2015).

## Acknowledgements

This research was supported by the Leader Researcher Program (NRF-2019R1A3B2068083).

## Author contributions

The original concept was conceived by JWY and YSC. SHS, YSC, and JWY developed the theory. YSC, SHS, SL, and MK performed the experiment. All authors discussed the result. JWY, YSC, and SHS wrote the manuscript.

## Competing interests

The authors declare no competing interests.

## Additional information

**Supplementary information** The online version contains supplementary material available at <https://doi.org/10.1038/s42005-024-01740-4>.

**Correspondence** and requests for materials should be addressed to Jae Woong Yoon.

**Peer review information** *Communications Physics* thanks Xingwei Gao, Chen Qian and the other, anonymous, reviewer(s) for their contribution to the peer review of this work. A peer review file is available.

**Reprints and permissions information** is available at <http://www.nature.com/reprints>

**Publisher's note** Springer Nature remains neutral with regard to jurisdictional claims in published maps and institutional affiliations.

**Open Access** This article is licensed under a Creative Commons Attribution-NonCommercial-NoDerivatives 4.0 International License, which permits any non-commercial use, sharing, distribution and reproduction in any medium or format, as long as you give appropriate credit to the original author(s) and the source, provide a link to the Creative Commons licence, and indicate if you modified the licensed material. You do not have permission under this licence to share adapted material derived from this article or parts of it. The images or other third party material in this article are included in the article's Creative Commons licence, unless indicated otherwise in a credit line to the material. If material is not included in the article's Creative Commons licence and your intended use is not permitted by statutory regulation or exceeds the permitted use, you will need to obtain permission directly from the copyright holder. To view a copy of this licence, visit <http://creativecommons.org/licenses/by-nc-nd/4.0/>.

© The Author(s) 2024